Preprint Title	Coordination-assembled Nanoarchitectonics of Antioxidant Peptide and Flavonoid Myricetin for Sustainably Scavenging Free Radicals
Authors	Xiaoyan Ma, Haoning Gong, Kenji Ogino, Xuehai Yan and Ruirui Xing
Publication Date	11 Jan. 2022
Article Type	Full Research Paper
Supporting Information File 1	Supporting Information.docx; 208.1 KB
ORCID® iDs	Haoning Gong - https://orcid.org/0000-0003-1590-2042; Xuehai Yan - https://orcid.org/0000-0002-0890-0340

Coordination-assembled Nanoarchitectonics of Antioxidant Peptide and Flavonoid Myricetin for Sustainably Scavenging Free Radicals

Xiaoyan Ma [a,b], Haoning Gong [b], Kenji Ogino [a]*, Xuehai Yan [b,c], Ruirui Xing [b,c]*

[a] Graduate School of Bio-Applications and Systems Engineering, Tokyo University of Agriculture and Technology, Tokyo, Japan

[b] State Key Laboratory of Biochemical Engineering, Chinese Academy of Sciences, Institute of Process Engineering, Beijing, P. R. China

[c] School of Chemical Engineering, University of Chinese Academy of Sciences, Beijing, P. R. China

Email: kogino@cc.tuat.ac.jp; rrxing@ipe.ac.cn

Graphic abstract:

Abstract

Oxidative stress can lead to permanent and irreversible damage for cellular components, and even cause cancer and many diseases. Therefore, the development of antioxidative reagents is a significant strategy for alleviating chronic diseases and maintaining the redox balance. Small-molecule bioactive compounds have exhibited huge therapeutic potential in antioxidant and anti-inflammatory. Myricetin (Myr) as well-defined natural flavonoid, has drawn wide attention on highly effective antioxidant, anti-inflammatory, antimicrobial, and anticancer activities. Especially at antioxidation, Myr is capable of not only chelating intracellular transition metal ions for removing reactive oxygen species (ROS), but also activating antioxidant enzymes and related signal, achieving sustainable scavenging radical activity. However, Myr possesses poor water solubility, which limits its bioavailability for biomedical application, even clinical therapeutic potential. The endogenous antioxidant peptide glutathione (GSH) plays a direct role on antioxidant in cells and possesses good hydrophilicity and biocompatibility, but is easily metabolized by enzyme. To take advantages of their antioxidation activity and overcome the above-mentioned limitations, the GSH, Zn^{2+} and Myr are selected to co-assemble into $Myr\text{-}Zn^{2+}\text{-}GSH$ (abbreviated as MZG nanoparticles or nanoarchitectonics). Thence, this study offers a new design to harness stable, sustainable antioxidant nanoparticles with high loading capacity and bioavailability, good biocompatibility for optimizing antioxidant to protect cells from oxygenated damage.

Keywords: Antioxidant, Co-assembly, Glutathione, Myricetin, Nanoarchitecnotics

1. Introduction

Oxidative stress caused by imbalance between the antioxidative and oxidative systems, leads to permanent and irreversible damage for cellular components, such as, proteins, lipids, and nucleic acids [1]. Furthermore, oxidative stress further leads to human diseases including Alzheimer's disease [2], cardiac disease [3], atherosclerosis [4], kidney disease [5], sepsis [6], cancer [7], and related inflammatory diseases

(periodontal disease, inflammatory bowel disease and *et al.*) [8,9]. Therefore, the development of antioxidative reagents is a crucial strategy for alleviating chronic diseases and maintaining the redox balance.

Increasingly high-efficient antioxidant materials are used for effectively scavenging multiple ROS. Reported metal-based nanomaterials such as CeO_2 and Fe_3O_4, have been widely applied for antioxidant therapy owing to admirable antioxidant activity [1,10]. Moreover, bioactive small-molecule compounds such as bilirubin and curcumin, antioxidant peptides such as glutathione and casein phosphopeptides, have exhibited huge therapeutic potential in antioxidant treatments [11-13]. Nevertheless, a plenty of disadvantages restrict bioapplication, including low biocompatibility of metal-based nanomaterials, low bioavailability of hydrophobic small-molecule compounds and easy degradation of antioxidant peptides by proteases. Current strategies of formulating with many carried materials, such as liposomes or polymer, have been reported. For example, PEG-modified liposomes loading resveratrol, layer-by-layer-coated gelatin nanoparticles, Gelucire-based solid lipid and polymeric micelles [14-19]. However, inducing low loading efficiency, systemic toxicity and tedious preparation process hinder bioapplication benefits.

Myricetin (Myr) as well-defined natural flavonoid, has drawn wide attention on highly effective antioxidant for anti-inflammatory, antimicrobial, and anticancer activities [16]. Especially in anti-inflammatory, Myr is capable of not only chelating intracellular transition metal ions for removing ROS [20], but also activating antioxidant enzymes and AMPK/NRF2 signal [21], achieving sustainable scavenging radical activity. It can inherently increase body resistance to carcinogens, viruses, and allergens, which is favorable for overall health [17]. In spite of tremendous potential, Myr possesses the same shortcomings as many hydrophobic small-molecules, including low bioavailability, poor water solubility and rapid degradation at pH > 6.8, which limits its clinical therapeutic potential [22]. Additionally, GSH is consisted of glycine, cysteine, and glutamic acid, whilst the cysteine residue plays a pivotal role in protecting the body from oxidation damage, but is easily metabolized by enzyme [23]. In this work, we employed a facile co-assembly strategy to design hybrid

nanoparticles for antioxidants [24-28]. Myr, Zn^{2+} and GSH were co-assembled to the Myr-Zn^{2+}-GSH nanoparticles (denoted as MZG nanoparticles). The obtained MZG possessed high loading capacity, good bioavailability and biocompatibility, achieving stable, durable and maximizing antioxidant effects.
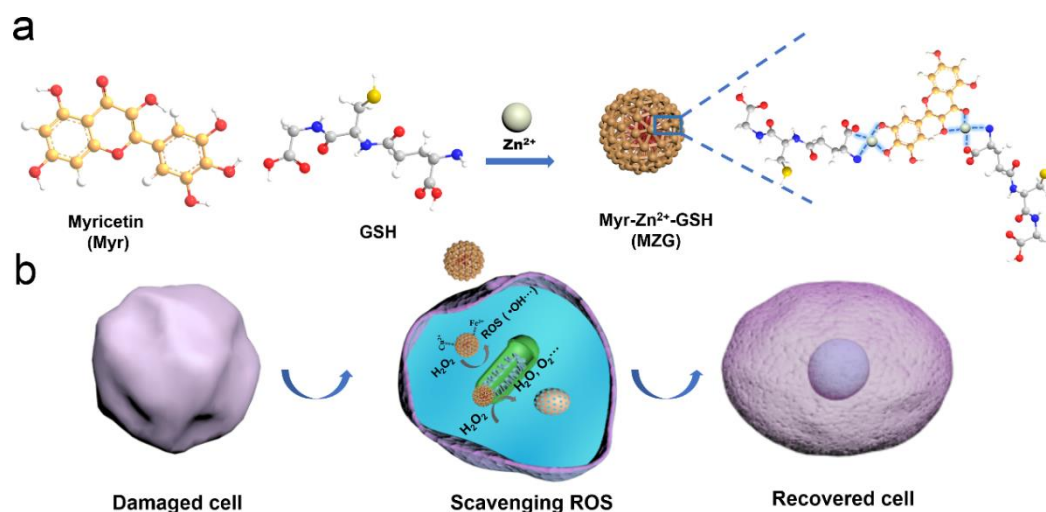
Scheme 1. Schematic illustration of preparing MZG nanoparticles (a) and antioxidation mechanism in cells (b). Noting that MZG nanoparticles afforded antioxidant activity for maintaining redox homeostasis in cells.

2. Experimental section

2.1 Synthesis of the MZG.

10 mg mL^{-1} of Myr was dispersed in 0.1 M NaOH, 10 mg mL^{-1} of GSH was dispersed in deionized water and 100 mM of Zn^{2+} was prepared. MZG nanoparticles were produced by 100 µL of Myr added into the mixed solution of 200 µL of GSH, 12.3 µL of Zn^{2+} and 684 µL of water. The Myr solution should be freshly prepared for use due to precipitation. The freshly prepared MZG nanoparticles were aged for 24 h at room temperature and placed in the dark. As-obtained nanoparticles were concentrated and purified by centrifugation, which were further used for other experiments.

2.2 Evaluation of ROS scavenging activity.

Firstly, the ABTS solution was prepared. 7 mM of ABTS aqueous solution was mixed with 2.45 mM of potassium persulfate aqueous solution equivalently and kept

them for 12 h in the dark. The UV/vis absorption intensity of ABTS solution (0.7 mM) was 0.7±0.02 through PBS dilution. A certain volume of diluted ABTS solution was added into different concentrations of Myr, GSH and MZG. A UV/vis spectrophotometer was used to record the absorption intensity of ABTS at 734 nm. The radical scavenging rate was calculated according to the following equation:

$$Scavenging\ rate\ (\%) = \frac{Abs\ @734nm\ ,control\ - Abs\ @734nm\ ,sample}{Abs@734nm\ ,control} \times 100\%$$

MZG nanoparticles and Myr/GSH complex were dispersed in H_2O for 5 days. Diluted ABTS solution was added with the same concentration of MZG and Myr/GSH complex (equivalent concentration of Myr and GSH: 4 µg mL^{-1}, 8 µg mL^{-1}) every day. UV/vis spectrophotometer was used for measuring the absorption intensity of ABTS at 734 nm. Then, the radical scavenging rate was calculated.

MZG suspension (equivalent concentration of Myr and GSH: 4 µg mL^{-1}, 8 µg mL^{-1}) and H_2O were added with ABTS aqueous solution. UV/vis spectra and the absorption intensity at 734 nm were recorded. The absorption intensity of ABTS at 734 nm was measured after 24 h. The same test method lasted for 5 days.

As-made MZG nanoparticles were acquired by centrifugation. Then MZG nanoparticles were incubated with different concentrations of H_2O_2 (0.01, 0.1, 1, 10, 100 mM). UV/vis spectrophotometer and dynamic light scattering were used to record absorption spectra and size change.

2.3 Cytotoxicity experiment in vitro.

The cytotoxicity of the as-made MZG was assessed against 3T3 cells. 3T3 cells were incubated by the different concentrations of MZG (equivalent concentration of Myr: 0, 10, 20, 40, 80 and 100 µM) for 24 h. The cell viability was tested by methyl thiazolyl tetrazolium (MTT) assay.

2.4 ROS scavenging activity evaluation in cells.

Firstly, the median lethal dose (LD50) value of H_2O_2 was evaluated. H_2O_2 at different concentrations (0, 10, 20, 40, 60, 80, 100, 150, 200 µM) were incubated with 3T3 cells. Secondly, ROS scavenging activity of MZG was further evaluated. After 3T3 cells treated by different concentrations of MZG for 24 h, 100 µM of H_2O_2 was

used to treat 3T3 cells. The capability of protecting cells from damage was accessed by cell viability. After the same method was employed, DCFH-DA was used to incubate these cells for 5 min, the fluorescence intensity of cells was recorded via confocal laser scanning microscope.

3. Results and discussion

3.1 Synthesis and characterization of MZG.

We selected a typical essential metal element Zn^{2+} as the coordination to Myr and GSH owing to effectively bonding both Myr and GSH via coordination interaction (Myr: GSH=2:1). The nanoparticles were formed by coordination self-assembly of Zn^{2+}, Myr and GSH (**Scheme 1a**). They were expected to show good antioxidant activity to protect cells from the ROS-induced damages (**Scheme 1b**). As shown in **Fig. 1a**, the transmission electron microscopy (TEM) image exhibited spherical MZG nanoparticles. The size and zeta potential value of MZG were 44.6±26.5 nm and -23.1±3.4 mV measured by dynamic light scattering (DLS) (**Fig. 1b**), which was consistent with TEM image. The UV/vis absorption spectra of pure Myr dispersed in 0.1M NaOH (pH=13), Myr/Zn^{2+} complex (pH=5.5) and MZG (pH=5.5) was detected by a UV spectrophotometer. Additionally, the UV/vis absorption spectrum of the MZG at 550 nm exhibited the blue shift compared with Myr-Zn^{2+}, which assigned to the charge transfer between GSH and Zn^{2+}(**Fig. 1c**). These results demonstrated that Zn^{2+} as the coordination component could co-assemble with Myr and GSH. Fourier transform infrared (FTIR) spectra were used to further confirm the self-assembly of MZG. In **Fig. 1d**, the two bands at 2522 cm^{-1} and 3350 cm^{-1} were mercapto group (-SH) and the stretching vibration of amino group (-NH_2) of GSH. The band at 1619 cm^{-1} was C=C group of Myr.
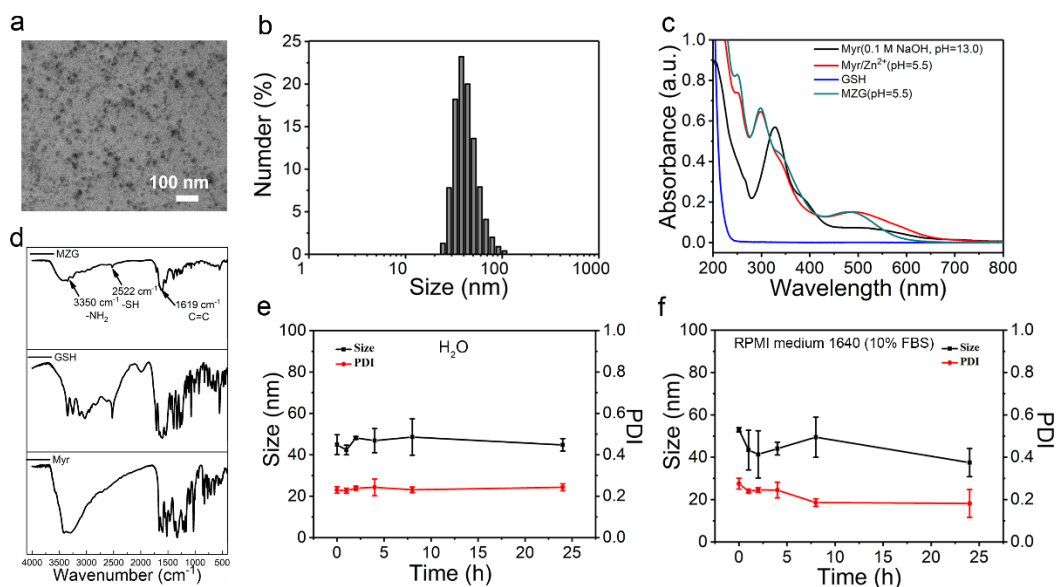
Fig. 1. Physicochemical characterization of MZG nanoparticles. (a) TEM image. (b) DLS profile of MZG nanoparticles. (c) UV/vis absorbance spectra of Myr dissolved in (0.1 M NaOH), Myr/Zn^{2+} complex, GSH and MZG (equivalent concentration of Myr: 20 µg mL^{-1}). (d) FTIR spectra of MZG, GSH and Myr. (e) Stability evaluation of MZG during incubation in aqueous solution at 37 °C for 24 h. (f) Stability evaluation of MZG during incubation in the 10% (v/v) RPMI medium 1640 basic at 37 °C for 24 h (equivalent concentration of Myr: 0.5 mg mL^{-1}).

The co-assembly approach overcame the poor water solubility of Myr and improved its bioavailability for further bioapplication. The stability of co-assembled nanoparticles was important for antioxidant application. DLS profile was used to evaluate the stability of MZG nanoparticles. The MZG nanoparticles (0.5 mg mL^{-1}) were either dispersed in water or diluted in RPMI medium 1640 containing 10% (v/v) fetal bovine serum (FBS) by 10-fold (v/v) at 37 °C for 24 h to investigate stability, respectively. The change of DLS was recorded at different time points (0, 2, 4, 8, 24, 48 and 72 h), showing that the average size and size distribution were not altered over time (**Fig. 1e, f**). The results indicated that MZG nanoparticles were stable in water and culture medium. Although noncovalent interactions are relatively weak compared to covalent interactions, the metal coordination interaction is the strongest

noncovalent interaction [4]. Hence, such interactions assured the stability of assembled nanoparticles in physiological conditions.
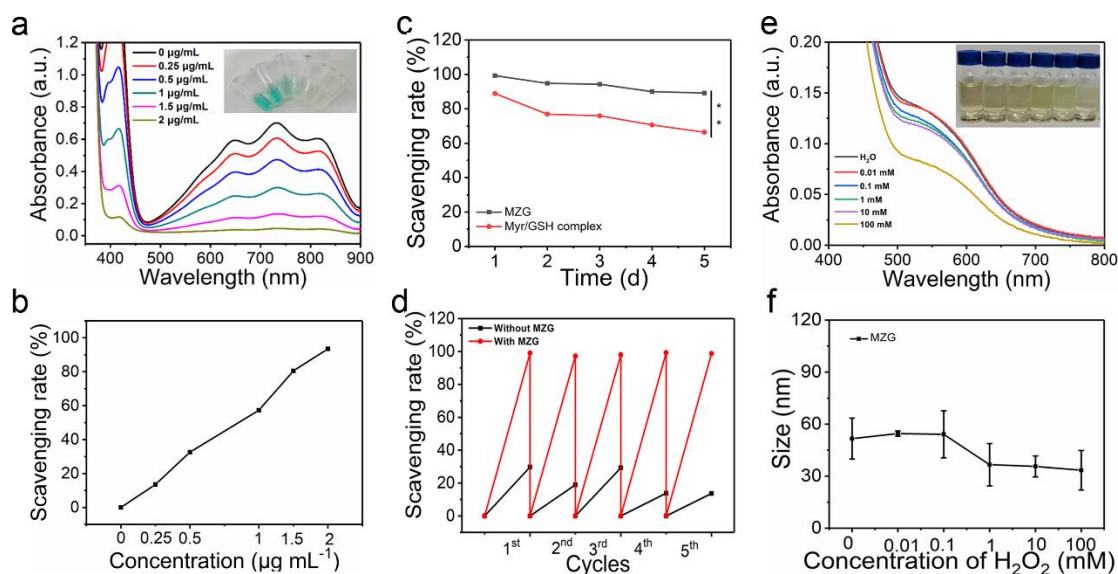
Fig. 2. ROS scavenging determination. a) UV/vis absorption spectra of ABTS solution incubated with different concentrations of MZG for 5 min (the sample picture shown in the inset, equivalent concentration of Myr: 0.25, 0.5, 1, and 2 µg mL^{-1}). b) The scavenging rate of MZG as fitted by maximum UV/vis absorption at 734 nm. c) Stably scavenging radical activity evaluation of MZG and Myr/GSH complex (equivalent concentration of Myr: 4 µg mL^{-1}, ** indicates p < 0.01). d) Sustainable radical scavenging activity evaluation of MZG (equivalent concentration of Myr: 4 µg mL^{-1}). e) UV/vis absorption spectra of MZG treated with different concentrations of H$_2$O$_2$ (equivalent concentration of Myr: 20 µg mL^{-1}). f) Size of MZG treated with different concentrations of H$_2$O$_2$ (equivalent concentration of Myr: 0.5 mg mL^{-1}).

3.2 Evaluation of ROS scavenging activity.

Myr possesses excellent antioxidant activity to scavenge ROS, which attributes to chelate metal ions like Fe^{2+} and Cu^{2+}, inhibits glutathione reductase activity and regulates of PI3K/Akt and MAPK signal pathways to avoid oxidative stress-induced apoptosis [20,29-32]. Moreover, GSH acts as an important antioxidant in the body owing to the reducibility of -SH. GSH is a non-enzymatic antioxidant molecule,

which is necessary for cell redox homeostasis and survival [33].

In this work, the 2, 2′-azino-bis (3-ethylbenzothiazoline-6-sulfonic acid) (ABTS) assay was employed to evaluate the radical scavenging activity [34]. The UV−vis absorption intensity of ABTS solution (0.7 mM) was 0.7±0.02 through phosphate-buffered saline (PBS) dilution. The diluted ABTS solution was incubated with GSH, Myr and MZG for accessing radical scavenging activity. The diluted ABTS solution was incubated with different concentrations of Myr (0.5, 1, 2, 3, and 4 μg mL^{-1}) for 5 min. The color of diluted ABTS solution gradually disappeared with increasing Myr concentration (**Fig. S1a**). After 5 min, the color of diluted ABTS solution completely disappeared, the scavenging rate of pure Myr at 4 μg mL^{-1} was up to 94.0% (**Fig. S1b**). The same way was used to evaluate scavenging rate of GSH. The ABTS solution was treated with different concentration of GSH (1, 2, 4, 6, and 8 μg mL^{-1}), showing that the color gradually disappeared (**Fig. S1c**). **Fig. S1d** exhibited that the scavenging rate of GSH at 8 μg mL^{-1} was up to 93.3%. **Fig. 2a** showed UV/vis absorbance of diluted ABTS solution incubated with different concentrations of MZG (equivalent concentration of Myr: 0.25, 0.5, 1, 1.5 and 2 μg mL^{-1}, equivalent concentration of GSH: 1, 2, 3, and 4 μg mL^{-1}) gradually decreased, suggesting that MZG nanoparticles scavenged radicals. When the concentration of MZG nanoparticles contained 2 μg mL^{-1} of Myr and 4 μg mL^{-1} of GSH, the scavenging rate of MZG was up to 93.5% (**Fig. 2b**). It demonstrated that the scavenging effect of co-assembled MZG nanoparticles was identical with Myr/GSH complex, indicating that co-assembly did not affect the ROS scavenging activity of Myr and GSH. As MZG nanoparticles could not only scavenge ROS, but also overcome the poor water-solubility of Myr, the co-assembly was effective to enhance bioavailability of both Myr and GSH, especially taking into account the sustainable antioxidant capability. The stable radical scavenging activity of MZG was further assessed. As shown in **Fig. 2c,** the radical scavenging activity of Myr/GSH complex was lower than that of MZG at the same concentration for 5 days, which demonstrated that MZG nanoparticles were more stable to scavenge radicals than Myr/GSH complex. Next, we explored weather as-obtained MZG possessed the sustainability of radical

scavenging activity owing to co-assembly that enhanced the stability of Myricetin and GSH. As shown in **Fig. 2d,** MZG performed the prolonged activity for scavenging radicals with addition of ABTS radicals compared with H_2O added ABTS radicals every day. It demonstrated that the as-obtained MZG exhibited stable and sustainable radical scavenging activity, which was favorable for further application.

ROS-responsive disruption of MZG during ROS scavenging was further explored. When MZG nanoparticles were used to incubate with different concentrations of H_2O_2 (0.01, 0.1, 1,10, 100 mM), UV/vis absorption spectra and sizes of MZG were measured. UV/vis absorbance of MZG at 550 nm (**Fig. 2e**) decreased with the increase of H_2O_2 concentrations. Then, the size of MZG was tested by DLS. The result showed that the size was also decreased dramatically with the increase of concentration of H_2O_2, indicating that MZG generated ROS-responsive disassembly (**Fig. 2f**).

3.3 Cell experiments.

The cytotoxicity of antioxidants is of importance for the biomedical applications. Therefore, the cytotoxicity of MZG was assessed by incubating with 3T3 cells, and the cell viability was determined via MTT assay [37]. 3T3 cells were treated by different concentrations of MZG (equivalent concentration of Myr: 10, 20, 40, 80 and 100 µM) for 24 h, exhibiting that the lowest cell viability was approximately 80% at the highest tested MZG concentration (**Fig. 3a**). The result indicated that MZG did not affect the growth of 3T3 cells.

The antioxidant activity of MZG was further examined using 3T3 cells through a MTT assay. As H_2O_2 could produce ROS, high level ROS could cause damage to cellular normal functions and components [35,36]. To explore the antioxidative effect of MZG, the LD50 value of 3T3 cells to H_2O_2 was measured by MTT assay. The cell viability of 3T3 cells was decreased with the increase of H_2O_2 concentrations (**Fig. 3b**). The result revealed that the LD50 concentration of H_2O_2 against 3T3 cells was 100 µM. Next, cell recovery due to the antioxidant activity of MZG was also demonstrated by MTT assay. After incubated with different concentrations of MZG (equivalent concentration of Myr: 2.5, 5, 10, 20, 40, 80 µM) for 24 h, 3T3 cells were

further incubated with 100 µM of H_2O_2 for 24 h. The cell viability was gradually increased with the increasing MZG concentration (**Fig. 3c**).
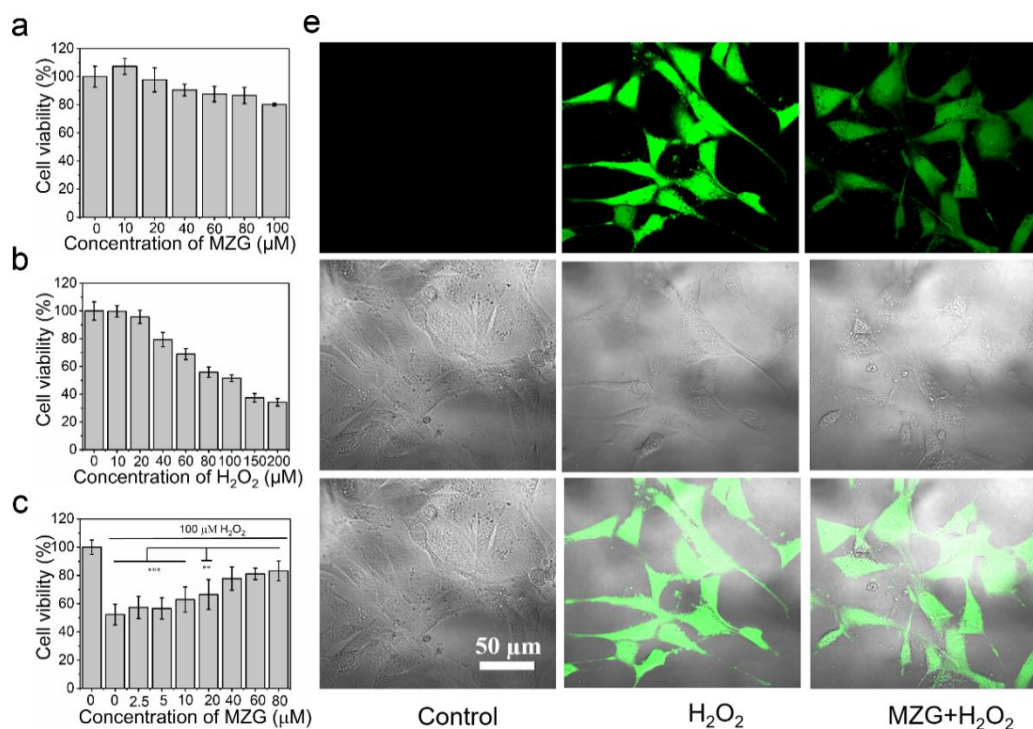
Fig. 3. Antioxidant activity evaluation in cells. a) Cytotoxicity evaluation of MZG by incubating 3T3 cells with different concentrations of MZG (equivalent concentration of Myr:10, 20, 40, 80 and 100 µM). b) H_2O_2-induced oxidative stress by incubating 3T3 cells with different concentrations of H_2O_2. c) Antioxidant activity evaluation of MZG using 3T3 cells under H_2O_2-induced oxidative stress (** indicates $p<0.01$, *** indicates $p<0.001$). d) CLSM images of 3T3 cells probed by DCFH-DA after incubating with MZG and H_2O_2 (the first row as fluorescence images, the second row as bright field images, and the third row as merged images).

This observation indicated that MZG could scavenge ROS to effectively protect cells from damage. Then, 2'7'-dichlorodihydrofluorescein diacetate (DCFH-DA) was used to probe ROS in cells, which showed no fluorescence signal without ROS, whilst turned to highly fluorescent 2'7'-dichlorofluorescein after interacting with ROS in cells. As shown in the confocal laser scanning microscopy (CLSM) images, the fluorescence intensity of cells treated by H_2O_2 and MZG was weaker than those only

11

treated by H_2O_2 (**Fig. 3d**), suggesting that MZG were capable of scavenging ROS in cells.

4. Conclusion

We have prepared antioxidant nanoparticles (MZG) by co-assembly of naturally occurring flavonoid Myr and endogenous antioxidant GSH in combination with metal ions. The resulting MZG nanoparticles overcame the disadvantages of water-insoluble Myr and fast metabolized GSH, improving their bioavailability. Importantly, the as-prepared MZG nanoparticles exhibited robust stability and sustainable ROS-scavenging activity, protecting cells from damage of ROS. The MZG nanoparticles with improved performances provide an alternative opportunity for optimizing antioxidation capability of conventional drugs, and present great potential for further biomedical applications.

5. Acknowledgements

References

[1] Z. Wei, L. Wang, C. Tang, S. Chen, Z. Wang, Y. Wang, J. Bao, Y. Xie, W. Zhao, B. Su, C. Zhao, Metal-Phenolic Networks Nanoplatform to Mimic Antioxidant Defense System for Broad-Spectrum Radical Eliminating and Endotoxemia Treatment, Adv. Funct. Mater. 30 (2020), 2002234.

[2] A. Herring, M. Blome, O. Ambrée, N. Sachser, W. Paulus, K. Keyvani, Reduction of Cerebral Oxidative Stress Following Environmental Enrichment in Mice with Alzheimer-like Pathology, Brain Pathol. 20 (2010), 166-175.

[3] J. Han, Y.S. Kim, M.Y. Lim, H.Y. Kim, S. Kong, M. Kang, Y.W. Choo, J.H. Jun, S. Ryu, H.Y. Jeong, J. Park, G.J. Jeong, J.C. Lee, G.H. Eom, Y. Ahn, B.S. Kim, Dual Roles of Graphene Oxide To Attenuate Inflammation and Elicit Timely

Polarization of Macrophage Phenotypes for Cardiac Repair, ACS Nano. 12 (2018), 1959-1977.

[4] Y. Wang, L. Li, W. Zhao, Y. Dou, H. An, H. Tao, X. Xu, Y. Jia, S. Lu, J. Zhang, H. Hu, Targeted Therapy of Atherosclerosis by a Broad-Spectrum Reactive Oxygen Species Scavenging Nanoparticle with Intrinsic Anti-inflammatory Activity, ACS Nano. 12 (2018), 8943-8960.

[5] D. Liu, E.J. Cornel, J. Du, Renoprotective Angiographic Polymersomes, Adv. Funct. Mater. 31 (2020), 2007330.

[6] M. Soh, D.W. Kang, H.G. Jeong, D. Kim, D.Y. Kim, W. Yang, C. Song, S. Baik, I.Y. Choi, S.K. Ki, H.J. Kwon, T. Kim, C.K. Kim, S.H. Lee, T. Hyeon, Ceria-Zirconia Nanoparticles as an Enhanced Multi-Antioxidant for Sepsis Treatment, Angew. Chem. Int. Ed. Engl. 56 (2017), 11399-11403.

[7] L. Zhao, Q. Zou, X. H. Yan, Self-Assembling Peptide-Based Nanoarchitectonics, Bull Chem. Soc. Jpn. 92 (2019), 70-79.

[8] X. Bao, J. Zhao, J. Sun, M. Hu, X. Yang, Polydopamine Nanoparticles as Efficient Scavengers for Reactive Oxygen Species in Periodontal Disease, ACS Nano. 12 (2018), 8882-8892.

[9] A. Nishiguchi, T. Taguchi, Oligoethyleneimine-Conjugated Hyaluronic Acid Modulates Inflammatory Responses and Enhances Therapeutic Efficacy for Ulcerative Colitis, Adv. Funct. Mater. 31 (2021), 2100548.

[10] S. Zhao, Y. Li, Q. Liu, S. Li, Y. Cheng, C. Cheng, Z. Sun, Y. Du, C.J. Butch, H. Wei, An Orally Administered CeO2@Montmorillonite Nanozyme Targets Inflammation for Inflammatory Bowel Disease Therapy, Adv. Funct. Mater. 30 (2020), 2004692.

[11] D.D. Kitts, Antioxidant properties of casein-phosphopeptides, Trends Food Sci. Technol.16 (2005), 549-554.

[12] C.H. Chung, W. Jung, H. Keum, T.W. Kim, S. Jon, Nanoparticles Derived from the Natural Antioxidant Rosmarinic Acid Ameliorate Acute Inflammatory Bowel Disease, ACS Nano. 14 (2020), 6887-6896.

[13] Y. Li, Q. Zou, C. Yuan, S. Li, R. Xing, X. Yan, Amino Acid Coordination Driven

Self-Assembly for Enhancing both the Biological Stability and Tumor Accumulation of Curcumin, Angew. Chem. Int. Ed. Engl. 57 (2018), 17084-17088.

[14] Z. Ahmadi, R. Mohammadinejad, M. Ashrafizadeh, Drug delivery systems for resveratrol, a non-flavonoid polyphenol: Emerging evidence in last decades, J Drug Deliv. Sci. 51 (2019), 591-604.

[15] T.G. Shutava, S.S. Balkundi, P. Vangala, J.J. Steffan, R.L. Bigelow, J.A. Cardelli, D. O'Neal, Y.M. Lvov, Layer-by-Layer-Coated Gelatin Nanoparticles as a Vehicle for Delivery of Natural Polyphenols, ACS Nano. 3 (2009), 1877-1885.

[16] F. Sun, Z. Zheng, J. Lan, X. Li, M. Li, K. Song, X. Wu, New micelle myricetin formulation for ocular delivery: improved stability, solubility, and ocular anti-inflammatory treatment, Drug Deliv. 26 (2019), 575-585.

[17] D.M. Gaber, N. Nafee, O.Y. Abdallah, Myricetin solid lipid nanoparticles: Stability assurance from system preparation to site of action, Eur. J Pharm. Sci. 109 (2017), 569-580.

[18] S. Battista, P. Campitelli, L. Galantini, M. Köber, G. Vargas-Nadal, N. Ventosa, L. Giansanti, Use of N-oxide and cationic surfactants to enhance antioxidant properties of (+)-usnic acid loaded liposomes, Colloid and Surface A. 585 (2020), 124154.

[19] M. Chatzidaki, I. Kostopoulou, C. Kourtesi, I. Pitterou, S. Avramiotis, A. Xenakis, A. Detsi, β-Cyclodextrin as carrier of novel antioxidants: A structural and efficacy study, Colloid and Surface A. 603 (2020), 125262

[20] G. Gupta, M.A. Siddiqui, M.M. Khan, M. Ajmal, R. Ahsan, M.A. Rahaman, M.A. Ahmad, M. Arshad, M. Khushtar, Current Pharmacological Trends on Myricetin, Drug Res (Stuttg). 70 (2020), 448-454.

[21] X. Kan, J. Liu, Y. Chen, W. Guo, D. Xu, J. Cheng, Y. Cao, Z. Yang, S. Fu, Myricetin protects against H2 O2 -induced oxidative damage and apoptosis in bovine mammary epithelial cells, J Cell Physiol. 236 (2021), 2684-2695.

[22] Y. Yao, G. Lin, X. Yan, P. Ma, T. Wu, Preformulation studies of myricetin: A natural antioxidant flavonoid, Pharmazie. 69 (2014) 19-26.

[23] A. Sharma, S. Kharb, S.N. Chugh, R. Kakkar, G.P. Singh, Effect of glycemic control and vitamin E supplementation on total glutathione content in non-insulin-dependent diabetes mellitus, Ann. Nutr. Meta. 44 (2000), 11-13.

[24] R. Xing, Q. Zou, C. Yuan, L. Zhao, R. Chang, X. Yan, Self-Assembling Endogenous Biliverdin as a Versatile Near-Infrared Photothermal Nanoagent for Cancer Theranostics, Adv. Mater. 31 (2019), 1900822.

[25] M. Cao, R. Xing, R. Chang, Y. Wang, X. Yan, Peptide-coordination self-assembly for the precise design of theranostic nanodrugs, Coord. Chem. Rev. 397 (2019), 14-27.

[26] Y. Liu, L. Zhao, G. Shen, R. Chang, Y. Zhang, X. Yan, Coordination self-assembly of natural flavonoids into robust nanoparticles for enhanced in vitro chemo and photothermal cancer therapy, Colloid and Surface A. 598 (2020), 124805.

[27] H. Sun, S. Li, W. Qi, R. Xing, Q. Zou, X. Yan, Stimuli-responsive nanoparticles based on co-assembly of naturally-occurring biomacromolecules for in vitro photodynamic therapy, Colloid and Surface A. 538 (2018), 795-801.

[28] R. Xing, C. Yuan, S. Li, J. Song, J. Li, X. Yan, Charge-Induced Secondary Structure Transformation of Amyloid-Derived Dipeptide Assemblies from beta-Sheet to alpha-Helix, Angew. Chem. Int. Ed. Engl. 57 (2018), 1537-1542.

[29] B.C. Dickinson, C.J. Chang, Chemistry and biology of reactive oxygen species in signaling or stress responses, Nat. Chem. Biol. 7 (2011), 504-511.

[30] N. Yahfoufi, N. Alsadi, M. Jambi, C. Matar, The Immunomodulatory and Anti-Inflammatory Role of Polyphenols, Nutrients. 10 (2018), 1618.

[31] D.K. Semwal, R.B. Semwal, S. Combrinck, A. Viljoen, Myricetin: A Dietary Molecule with Diverse Biological Activities, Nutrients. 8 (2016), 90.

[32] X. Li, W. Mai, D. Chen, Chemical Study on Protective Effect Against Hydroxyl-induced DNA Damage and Antioxidant Mechanism of Myricitrin, J Chin. Chem. Soc. 61 (2014), 383-390.

[33] C. Gorrini, I.S. Harris, T.W. Mak, Modulation of oxidative stress as an anticancer strategy, Nat. Rev. Drug Discov. 12 (2013), 931-947.

[34] D. Yim, D.E. Lee, Y. So, C. Choi, W. Son, K. Jang, C.S. Yang, J.H. Kim, Sustainable Nanosheet Antioxidants for Sepsis Therapy via Scavenging Intracellular Reactive Oxygen and Nitrogen Species, ACS Nano. 14 (2020), 10324-10336.

[35] H. Sies, D.P. Jones, Reactive oxygen species (ROS) as pleiotropic physiological signalling agents, Nat. Rev. Mol. Cell Biol. 21 (2020), 363-383.

[36] B. Yang, Y. Chen, J. Shi, Reactive Oxygen Species (ROS)-Based Nanomedicine, Chem. Rev. 119 (2019), 4881-4985.

[37] A. Mujagic, A. Marushima, Y. Nagasaki, H. Hosoo, A. Hirayama, S. Puentes, T. Takahashi, H. Tsurushima, K. Suzuki, H. Matsui, E. Ishikawa, Y. Matsumaru, A. Matsumura, Antioxidant nanomedicine with cytoplasmic distribution in neuronal cells shows superior neurovascular protection properties, Brain Res. 1743 (2020), 146922.